RIGA TECHNICAL UNIVERSITY

Faculty of Materialscience and Applied Chemistry

Institute of Technical Physics

Mārtiņš Vanags

PhD of Doctoral study program "Materialsciences"

Synthesis and properties of nanostructured iron oxide photoanodes; mechanisms of the pulse electrolysis and photo-electrolysis

Summary of Doctoral Thesis

Scientific Advisors:

Dr. Sc. Ing. Andris Šutka

Dr. Phys. Jānis Kleperis

Riga 2015

Šis darbs izstrādāts ar Eiropas Sociālā Fonda atbalstu projektā „Inovatīvu funkcionāli materiālu un nanomateriālu izstrāde izmantošanai vidi kontrolējošās tehnoloģijās”. Nr. 2013/0010/1DP/1.1.1.2.0/13/APIA/VIAA/030

This work has been supported by the European Social Fund within the Project „Elaboration of Innovative Functional Materials and Nanomaterials for Application in Environment Control Technologies”, No 2013/0010/1DP/1.1.1.2.0/13/APIA/VIAA/030

Эта работа была поддержана Европейским социальным фондом в рамках проекта "Инновационные функциональные материалы и наноматериалы для использования в разработке технологий, которые контролируют окружающую среду», № 2013/0010 / 1DP / 1.1.1.2.0 / 13 / APIA / VIAA / 030

ISBN 978-9934-507-98-4

DOCTORAL THESIS

NOMINATED FOR PHYSICS DOCTORAL DEGREE AT RIGA TECHNICAL UNIVERSITY

Thesis for doctoral degree in physics will be publicly defended on June 3, 2015 at the Faculty of Material Science and Applied Chemistry, Riga Technical University, Paula Valdena Street 3/7, Auditorium No. 272.

OFFICIAL OPPONENTS

Professor, Dr.habil.phys. Uldis Rogulis
Institute of Solid State Physics, University of Latvia

Professor, Dr.habil.phys. Jānis Grabis
Institute of Inorganic Chemistry, Riga Technical University

Professor, Dr.habil.chem. Donāts Erts
Institute of Chemical Physics, University of Latvia

APPROVAL

I confirm that I have developed this thesis submitted to Riga Technical University for the doctoral degree in physics. This thesis has not been submitted to any other university degree.

Mārtiņš Vanags …….(Signature)

Data: ……

Full thesis is written in Latvian language, contains an introduction and 5 chapters; literature review, methodological part, results and discussion, overall conclusions, thesis to be defended and list of references, 87 drawings and illustrations, all-together 164 pages. The list of references contains 151 titles.

Content

GENERAL DESCRIPTION OF THE WORK

Introduction

Adding energy to split water produces the oxygen and hydrogen, burning of which in a stoichiometric ratio (with flame or chemically in the presence of a catalyst) gives energy and water - this cycle does not pollute the environment and do not spend resources of Earth. Of course, it is possible under condition where the energy for splitting of water comes from renewable resources - sun, wind, moving water power, biomass etc. Hydrogen is not only fuel but also an indispensable energy carrier to store energy obtained from renewables longer, cleaner and safest as in batteries. In near future the hydrogen will be used worldwide for balance of energy supply and zero-emission transport and power generation. In addition, the hydrogen can be found practically anywhere on Earth (mostly in compounds) and can be obtained from local resources, both fossil and renewable. The production of hydrogen from water by DC electrolysis method is known since the 19th century, and commercially launched at the beginning of the 20th century. Efficiency of industrial electrolyzers does not exceed 70%, and this is the main drawback of electrolytically produced hydrogen, because the price of it consists mostly of electricity costs. Does electrolysis can be made more effective? In 1956 world-famous creator of physical electrochemistry Bernhardt Patrick John O'Mara Bockris wrote that the pulse electrolysis is more efficient than conventional electrolysis. It has not been approved practically until now although many patents are issued and public forums are full with discussions.

Our studies of water electrolysis with pulses clarify that by providing pulse to the electrochemical cell, the voltage is first supplied to charge the electric double-layer boundary formed at electrode/electrolyte interface. An ionic (Faraday's) current starts flowing in the circuit after this charge has reached the value of over-voltage at which the water electrolysis reaction began. We demonstrated that at very short pulses the charging of the geometric capacitance of electrochemical cell can be separated from succeeding charging of double layer capacitance and final discharge in electrolysis. In addition, comparison of DC and pulse electrolysis is not easy, and empirical approach is developed to do it by means of volt-ampere curves approximations.

Electrodes from semiconductor materials to split water by photo-electrolysis are the second theme developed in this work. The ultimate goal of photo-electrolysis is to split the water with solar radiation by converting it in chemical energy, i.e., hydrogen. Such a method to produce hydrogen is extremely promising process due its simplicity and environmental reasons. Photolysis is being known for long ago, but researchers worldwide are still looking for efficient materials and robust methods to synthesize it.

One from the materials able to fulfill the requirements of efficient photo-electrode is alpha-phase ferric oxide (hematite α-Fe_2O_3). In stoichiometric mixture the hematite is an insulator, but typically it is non-stoichiometric material with oxygen vacancies, as a result is the change of electrical properties from insulator to semiconductor. Hematite is a non-toxic, stable in a wide pH range, cheap and with the proper width of the forbidden gap close to the maximum of visible solar radiation.

Overall, our work focuses on the pulse electrolysis, pulse plating techniques and research of electrode morphology, composition and photo-electrochemical properties for photo-anode materials in photolysis cell. Work is divided into three parts – research of water pulse electrolysis process on interface electrode/electrolyte, development and comparison of plating (DC voltage scan, pulse) and pyrolysis thin film coating methods to obtain optimal photo-anode material, and third – research and explanation of the role of yttrium impurity in hematite structure on the physical and chemical characteristics.

Status of the Problem

The voltage pulse generated in the inductive circuit to rapidly stopping current in it, is very short (below microsecond) and with high amplitude (up to thousands of volts) at open circuit conditions. If the load for inductive voltage pulse is water electrolysis cell, pulse kinetics changes significantly - two distinctly different parts can be separated: the rapid charging part followed by a long discharge tail. For such a drastic difference in the kinetics of pulse on electrolysis cell is not found unequivocal explanations in the scientific literature has been found jet; the pulse electrolysis process is little studied with the help of current-voltage characteristics. Empiric method is proposed in our work to determine the effective values of current and voltage in case of inductive pulses, avoiding necessity to solve Fick`s diffusion equation.

Hematite (α-Fe_2O_3) is one of the most studied anode material for splitting water in the photolysis process. For example, it is known that photo-electrical properties of α-Fe_2O_3 thin films depend on their composition, stoichiometry and microstructure. It is also known that characteristics of hematite thin films made in pulse galvanization process are significantly different comparing with films obtained in DC galvanization process. It is made alloying of hematite thin films with different impurity elements and explained their impact on the structure, morphology and physical-chemical properties.

Talking about impurities, impact of Y^{3+} ion on properties of hematite has not been studied yet and firstly is done in our work. Yttrium comes from transition metal group, with ion radius very different from the Fe^{3+} ion radius, and as an impurity in hematite structure will take place in the center of oxygen octahedron, and would significantly distort nearest oxygen octahedrons with iron ions in the center, affecting additional charge carriers (electrons and holes) generated by the light, their recombination and promoting separation of charge carriers, thereby increasing hematite photo-activity.

Pulse electrolysis theory and technology is widely used in metal galvanization, but little is known about thin film semiconductor materials obtained in pulse galvanization process. The scientific literature does not provide clear information on impact of pulse parameters during electrochemical plating process on the photo-electrochemical properties of obtained hematite thin films. In addition, despite the many advantages of hematite as photo-anode material for water splitting with light from the Sun, location of its valence and conduction bands do not scale the water oxidation-reduction potentials; the diffusion length of holes is very short (2-4 nm) visible light absorption depth is too large, what all-together promotes fast recombination of light-induced charges.

The Goal of Work

Goal is to decrease loses in water electrolysis process by studying the nature of short inductive voltage pulses on interface electrode/electrolyte, and to develop improved photo-anode material by elaborating innovative plating methods and composition.

The Tasks

1. To study the inductive voltage pulse kinetics of water electrolysis cell and develop a method to compare pulse electrolysis with the DC;
2. Explore and optimize the synthesis of hematite thin films by electrochemical plating method and compare its photo-electrochemical properties by coatings obtained with spray pyrolysis method;
3. Investigate the voltage pulse plating process to obtain hematite thin films properties; clarify the role of pulse parameters on the properties;
4. Identify the effect of yttrium impurity on photo-electrochemical and physical properties of Fe_2O_3 thin films.

Scientific Novelty

The practical significance of this work is determined with the increasing need for the best energy carrier to store unpredictable in time scale electricity from renewables (sun, wind), - hydrogen, which is available in compounds on Earth in many renewable resources – water, biomass. The main idea of Hydrogen Energy is to create a bridge between energy producers and energy consumers. If the energy is produced from renewable energy sources (wind, sun, water, etc.) and stored in the form of hydrogen to reach the consumer when needed, where it is converted back into electricity and/or heat in processes with zero emissions, then life cycle of this energy is completely ecological. Efficient water electrolysis and photolysis to produce the hydrogen from solar or wind energy is a contributing factor in the development of hydrogen energy.

Separation of capacitive charging process from the charge transfer process is carried out in an inductive voltage pulse water electrolysis process. Separation of both processes, in practice, allows to split water into hydrogen and oxygen in reversible process conditions that make the water electrolysis most efficient. Firstly study about the nature of inductive short voltage pulse on electrolysis cell with aqueous solution is performed; firstly microsensors are used to study the concentration of the dissolved hydrogen and oxygen near the electrodes in the process of pulse electrolysis

The synthesis of iron oxide thin film photo-anode electrodes with electrochemical pulse plating method is explained in depth and described the influence of pulse parameters on the photo-electrochemical properties of resulting material is described. Suggested several ways to improve the iron oxide coating photo-electrochemical properties of both - cathodic and anodic - plating processes, as well as of spray pyrolysis, using firstly yttrium as impurity element to improve photo-electrochemical properties of hematite (not described in the scientific literature).

CONTENT OF THE WORK

Literature Review

In this literature review it is revealed that pulse electrolysis is not widely described in the scientific literature, although Ghoroghchian and Bockris [1] in 1956 proposed that the pulse electrolysis is more effective than conventional electrolysis, and later huge amount of patents have been issued to several authors and companies. The water splitting scheme described in patents initiated a huge interest, but nobody has succeeded in interpreting this scheme and its performance mechanisms up to now, and what is more important, nobody has succeeded in experimentally repeating devices described as well [2]. The explanation of pulse electrolysis process and its significant effectiveness can not be found. There are few descriptions in the literature of this kind of electrolysis supply, and conclusion was that efficiency of pulse water electrolysis is not depending on the power supplied to electrolysis cell, thus being in contradiction to the conventional opinion of electrolysis [3]. When inductive voltage pulse is delivered to water electrolysis cell, two different processes appears after pulse kinetics: rapid charge followed by slow discharge. It is possible to conclude form the pulse kinetics that the double-layer charging process has been separated from the electrochemical reaction, which has not been mentioned nor analyzed in the previous researches [2]. To prove this we have done plenty of experiments proving charging process separation from the electrochemical water splitting reaction.

Equivalent circuit of electrochemical cell contains nonlinear circuit elements, so it is very likely that the pulsed electrolysis can improve the energy efficiency of the common water electrolysis process. Based on this assumption in a number of publications [3, 4] authors are seeking for the resonance frequency in circuit with electrochemical cell, thus achieving energy efficiency gains only of 15%.

Summarizing it can be concluded that the voltage pulse applied to electric double-layer in electrode/electrolyte interface creates substantially different conditions as in the case of DC. It is possible to distinguish in electrical double-layer the part in which the concentration of active ion is pulsating, wherein the thickness of pulsating double-layer is inversely proportional to the pulse frequency and pulse current. Since the pulse frequency and the current both are easy to be increased with the modern pulse generators, it can be possibly to obtain especially low thickness of pulsating double-layer and perfectly cover nano-terrain unevenness. From this aspect such pulse coating process can be applied in nano-topography, using for electrochemical etching purposes with very low resolution.

A lot of researches are published about photo-electrical properties of various materials and their possible application for water splitting with visible light. It is shown that the hematite might be one of the more suitable, the most widely occurring and environmentally friendly material, unless the position of zones to be closer to the red-oxide reactions of water, as well as charge carrier (hole) diffusion path length would be larger and visible light absorption depth - less. Numerous studies made attempts to rectify these shortcomings, alloyed the hematite with various elements. In the full Thesis the review from literature about impact of alloying elements on structure, morphology and photo-activity of hematite is given. It was concluded that yttrium has not been studied as alloying element in hematite, also Y impurity

impact on photo-electrochemical properties of Fe_2O_3 is not studied. Yttrium is a transition metal ion with radius which is very different from the Fe^{3+} ion radius, and as an impurity in hematite structure it could distort the neighborhood oxygen octahedra with iron ions in the center. It can also affect the recombination of light-generated charge carries (holes and electrons) and encourage increase of photo-activity.

Methodological part

Self-made water electrolysis cell consisting of a cylindrical plexiglass shell and closed by caps both ends (Figure 1a) was used for inductive voltage pulse kinetics measurements. The upper lid of cell incorporates a stainless steel electrodes (wire with a diameter of 1.5 mm), which may change the spacing between them; lower lid incorporates outlet pipes to measure volume of discharge gases.

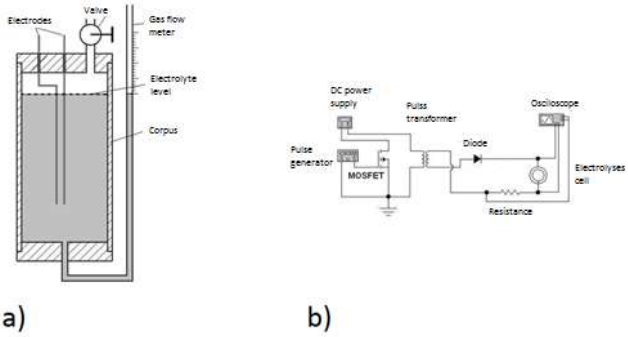

Figure 1. Water electrolysis cell used for measurements (a); the cheme to generate pulses (b).

The electrode area contacting with electrolyte - 2.8 cm^2; electrolytes used - 0.1M, 0.3M and 0,5M KOH solutions. At each spacing between electrodes (1mm, 3mm and 5mm) and each solution concentration the voltage and current pulses were recorded and impedance spectra measured.

Inductive voltage pulse generating circuit was formed (Figure 1b) from a DC power supply Agilent N5751A, pulse generator GFG-3015, IRF840 MOSFET semiconductor switch, pulse transformer, blocking diode, water electrolysis cells as load, benchmark resistivity and oscilloscope GDS-2204 .

Special cell was constructed to measure inductive voltage pulse electrolysis with electrodes from different materials and dissolved hydrogen concentration measurements in direct vicinity of the cathode. The cell consists of three separate chambers, which are connected to each other by an electrolyte bridge (Figure 2). The first chamber is for nickel plate counter-electrode; second chamber is for working electrode (platinum and tungsten wires with

diameter 0.5 mm and length 100 mm). As electrolyte 0.1 and 0.2 M KOH solutions were used.

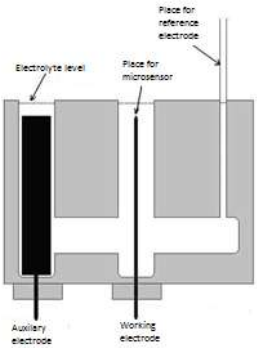

Figure 2. Water electrolysis cell to measure the concentration of dissolved hydrogen.

In order to assess the amount of hydrogen gas released from electrode and dissolved in the electrolyte, micro-sensor (Clark type sensor from Unisense, Denmark) was placed adjacent to electrode. The end of micro-sensor is 100 micrometers thick glass tube closed with a silicone membrane, and placed in 1 mm distance from the surface of electrode under study. The experiment has held as follows: separate inductive voltage pulses were fed to the electrolysis cell on which voltage and current oscillograms recorded. At the same time, concentration of dissolved hydrogen in solution is measured with micro-sensor to assess the amount of released hydrogen. The measurements were carried out over longer time periods and results integrated.

Popov [5] used effective values of pulsed current and over-voltage to compare pulsed electrolysis with DC electrolysis; over-voltage and current values were plotted changing the pulse amplitude, thus yielding volt-ampere (VA) characteristics, which can be compared to the resulting VA curve of DC mode. Effective values of current and over-voltage can be found using the following equation [5]:

$$i_{eff} = \frac{nFD}{T}\int_0^T \frac{\partial C}{\partial x}(0,t)dt \qquad (1)$$

$$\eta_{eff} = \frac{1}{T}\int_0^T \eta(t)dt \qquad (2)$$

where n - the number of elementary charges within the same elementary reaction step; F - Faraday's constant; D - Diffusion coefficient ions taking part in the reaction; T - pulse period; $\partial C / \partial x$ - concentration gradient in the x direction ions taking part in reactions (x direction is perpendicular to the plane of the electrode). The term i_{eff} in equation (1) is obtained from the concentration gradient, in turn to find the gradient, the Fick`s diffusion equation must be solved, which may complicate the task. In our work, the current in not calculated but

measured during the process, because the equation (1) can be simplified, yielding similar equation to the equation (2):

$$i_{eff} = \frac{\eta_I}{T}\int_0^T i(t)dt \qquad (3)$$

where η_I is a current efficiency of water electrolysis process.

Values of effective over-voltage and current are obtained from equations (2) and (3), changing the pulse amplitude and recording the values of voltage and current in time.

The electrolyte was prepared from deionized water and KOH in concentrations: 0.1M KOH, 0.3M KOH and KOH 0,5M; at each concentration kinetics of the process was studied in three distances: 1mm, 3mm and 5mm.

To find the effective current value from eguation (3) amount of released hydrogen gas must be determined, what we did using the extrusion method. At each point the gas amounts was measured 10 times, and then mean value found and the amount of gas and error estimated.

Several pulses with different amplitudes were recorded at one solution concentration and at the same distance between electrodes, and different effective values obtained using equations (2) and (3). V-A curve is obtained using these values and plotting them in plane V-A. At the same configuration of the electrodes and the concentration of the solution the DC volt-amperic curve is measured with VoltaLab PGZ 301 potentiostat in voltammetric cyclic mode: from -2,5V to + 2,5V with a scan rate of 50mV/s in two-electrode cell. Acquired DC Current-voltage characteristic were compared with the constructed pulse mode VA curves.

The spray pyrolysis method was used to obtain pure hematite α-Fe_2O_3 thin films and yttria doped hematite thin films $Y_xFe_{2-x}O_3$ where x=0.05, x=0.1, x= 0.15 and x = 0.2. Metal salt solution (precursor solution) is repeatedly sprayed on the heated substrate by help of carrier gas - nitrogen. Solution droplets collide with the hot base, and if not already evaporated, then gush over its surface, while reacting and thermally decomposing. Solution components are selected so that the reactants and final products, which do not fall within the intended composition of thin films, evaporate during this process [6].

The heater temperature control unit for spray pyrolysis system (Figure 3) consists from thermocouple Pt100, thermo-controller LUMO72, who heads the SSD relay that turns on or off the heater power. Precursor solution is sprayed with a pneumatic spraying system SIRA 06XT299 (Taiwan) coupled with nitrogen gas tank. In order to synthesize pure α-Fe_2O_3 the $FeCl_3 \cdot 6H_2O$ 0.1M solution in deionized water is prepared, but to get the yttria-substituted hematite $Y_xFe_{2-x}O_3$ thin layer, in addition 0.1M $YCl_3 \cdot 6H_2O$ solution in deionized water is being prepared and mixed in fixed-volume relationship (see Table 1) with ferric chloride solution and stirred for 1 h at room temperature. The prepared precursor solution is poured in reservoir of spray gun and at rate of 4 ml/min and pressure of carrier gas 2.5 bar is sprayed on the glass plate coated with the electro-conductive fluorine doped tin oxide (FTO) film. FTO/glass substrate was attached to the heater plates, covering 3mm from the upper part with aluminum foil (non-exposed area for photo-electrochemical measurements). The substrate is heated to 400 ° C at a rate of 10 ° C/min; spraying sequence of one cycle selected as follows:

0.5 seconds spraying, than 30 seconds pause (required for drops fallen on the hot pan to crystallize until the next spray cycle).

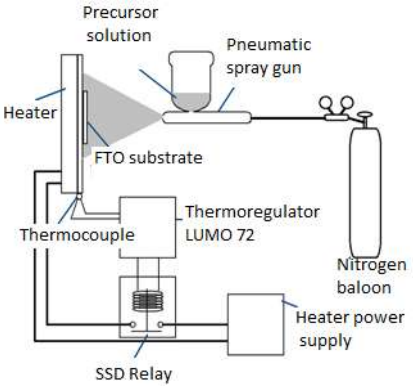

Figure 3. Spray pyrolysis stand scheme

Table 1. The proportions of precursor solutions to obtain necessary composition of layer.

Desired composition	$FeCl_3 \cdot 6H_2O$ 0,1M solution volume	$YCl_3 \cdot 6H_2O$ 0,1M solution volume
α-Fe_2O_3	20 ml	---
$Y_{0,05}Fe_{1,95}O_3$	19,5 ml	0,5 ml
$Y_{0,1}Fe_{1,9}O_3$	19 ml	1 ml
$Y_{0,15}Fe_{1,85}O_3$	18,5 ml	1,5 ml
$Y_{0,2}Fe_{1,8}O_3$	18 ml	0,2 ml

The substrate is heated to 400 ° C at a rate of 10 ° C/min; spraying sequence of one cycle selected as follows: 0.5 seconds spraying, than 30 seconds pause (required for drops on the hot pan to crystallize until the next spray cycle). It is possible to obtain films of different thicknesses while changing the number of spray cycles; in our work it was varied from 15 to 45 cycles. After spraying the substrate is slowly cooled down with speed 5 °C/min. The samples are then placed in an oven and burned at 500 ° C for 30 min, which is necessary for the coated material completely crystallized on the hematite phase. Oven-heating rate - 5 °C/min, following cooling took place naturally, together with turned off the oven.

Cathodic plating method was used to obtain pure hematite α-Fe_2O_3 thin films on the FTO/glass substrate (1.3 x 2.5 cm) from the plating solution 5mM $FeCl_3 \cdot 6H_2O$ + 5mM KF • $2H_2O$ + 0.1M KCl at 40 ° C in three electrode cell (12 cm^2 platinum sheet as a counter-

electrode and a standard saturated calomel electrode (SCE) as reference electrode) with potentiostat VoltaLab PGZ 301. 3 ml of 30% H_2O_2 were added to 30 ml plating solution before plating process start-up, to increase the total peroxide concentration of the working solution up to 1M.

Galvanization has two different modes: cycling potential (PC) mode and pulsed potential (PP) mode. In PC mode the potentiostat scanned potential between two values with rate of 20 mV/s. The values of final potential were changed to optimize galvanization parameters, but the best results were obtained when they were from 0 mV and to -200mV. In order to obtain different thicknesses of layers, the number of scanning cycles was changed, while the minimum was 15.

In PP mode during plating the potential was switched between two potential values, which corresponded to PC mode in order to later be able to compare the physical and photo-electrochemical properties of the resulting coatings. We tested two frequencies in PP mode: 0.25 Hz and 1 Hz.

Samples after the PC and PP plating were placed in an oven and heated 1 h at 450 ° C; heating rate from ambient temperature to 450 °C - 5 °C/min, cooling to room temperature naturaly with the furnace down to room temperature.

Anodic plating method was used to obtain pure hematite α-Fe_2O_3 thin films from plating solution $FeCl_2$ 0,02M at 75 °C on the FTO/glass substrate (1.3 x 2.5 cm), which served as the working electrode. Three electrode electrochemical cell was used with a 12 cm^2 platinum sheet as counter-electrode and SCE as a reference electrode and potentiostat VoltaLab PGZ 301. Like cathodic plating, also anodic was used in two different plating modes: potentiostatic and pulsating potential (PP). In the potentiostatic mode working electrode was supplied to +1200 mV potential and galvanization prolonged 10 min. In PP mode the potential switched between + 1200mV and 0 mV. Pulsation has a fill factor of 50% at two frequencies - 0.25 Hz and 1 Hz frequency. After plating the samples were placed in an oven and heated at 450 °C for 1 h, the oven warms up at a rate of 5 ° C/min and cooled down naturally.

The resulting material is characterized with different methods: the surface profilometry (thickness), X-ray diffraction phase analysis, scanning electron microscopy, X-ray photo-electron spectroscopy, optical properties and electrochemical impedance spectroscopy.

To realize photocurrent measurements we used self-made photo-electrochemical cell (Figure 4) of POM plastic with two perpendicular drilling. The round glass cell with electrolyte, working electrode (thin film on FTO/glass substrate), counter-electrode (Pt sheet 12 cm^2) and a reference electrode (SCE) is inserted into the vertical hole. An axis with electric motor at one end, and a light modulator on second was placed in plastic housing below the horizontal and the vertical holes. Light modulator consisted of metal sheet in the form of half of the circle, and with motor turning, horizontal drilling was periodically (2,5 rpm) closed and illuminate, creating periodical intervals of light and darkness. Cell was connected to potentiostat VoltaLab PGZ 301 and open circuit potential measured 30 minutes, followed by a photocurrent measurement during which the potentiostat in linear voltage cycling mode scanned voltage from -400 mV to + 400mV (2mV/s), thus recording volt-ampere curve. In

parallel to current-voltage characteristic modulator opened/closed the light from 30W LED projector (white light with radiation spectrum similar to the sun) periodically for 20 seconds, thereby ensuring almost simultaneous measurements of volt-amperic curves in darkness and in the light (potential scan is sufficiently slow). Characteristic photocurrent values of the sample are obtained by calculating the difference between current values in light and dark.

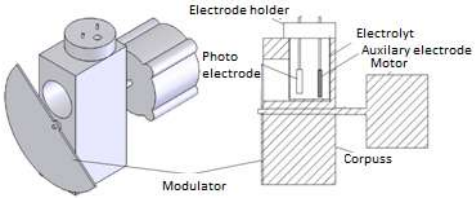

Figure 4. Construction of photo-electrochemical cell

Mott–Schottky curve was measured at fixed frequency 10 kHz by scanning the potential applied to electrochemical cell from -500 mV to + 200mV (increment 50 mV). Figure 5 shows Mott–Schottky plot obtained already with VoltaLab PGZ 301 potentiostat in fixed-frequency impedance mode. Also, Mott–Schottky equation is shown in Figure 4, where C - the barrier layer capacity, ε - relative dielectric permeability of semiconductor material, ε_0 - absolute dielectric permeability, A - area of the electrode, e - electron charge, N_D – concentration of charge carriers, E - the applied potential, E_{FB} - flat bond potential, k_B - Boltzmann constant, T - absolute temperature. By extrapolating the straight area in curve to zero and knowing the applied external potential value, the flat bond potential E_{FB} can be estimated.

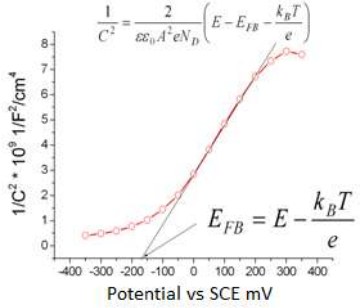

Figure 5. Example of Mott–Schottky plot and estimation of flat bond potential E_{FB}.

Charge carrier concentration N_D is determined from the slope k (equation 4) of curve in Mott-Schottky plot (Figure 5):

$$k = \frac{2}{\varepsilon\varepsilon_0 A^2 e N_D} \quad (4) \qquad \text{and accordingly } N_D: \quad N_D = \frac{2}{\varepsilon\varepsilon_0 A^2 e k} \quad (5)$$

Knowing the value of capacitance for a given potential, the barrier layer thickness can be determined using the following equation:

$$d = \frac{C}{\varepsilon\varepsilon_0 A}, \qquad (6)$$

where d is the thickness of the barrier layer, C - capacity. The barrier layer thickness in our work is calculated at 0V potential accordingly to SCE.

Results and discussion

Pulse electrolysis

Inductive voltage and current pulse kinetics of water electrolysis cell (Figure 6a) can be divided into two fundamentally distinct parts: a rapidly growing charging (1µs) and slowly descending discharge tail (about 20µs). The transition from the rapid charging to slow discharge tail happens through the breakpoint. By changing spacing between electrodes, the charging amplitude voltage pulse changes (Figure 6b) – at 5mm distance the rapid charging end at about 5V, while reducing the distance between the electrodes to 3mm and 1mm, the voltage value at the end of the charge drops to 4,2V and 3,8V respectively.

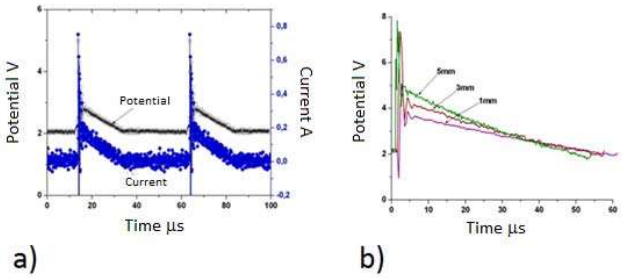

Figure 6. a) Typical voltage and current pulse kinetics of water electrolysis cell; b) Electrode spacing effect on the voltage pulse kinetics.

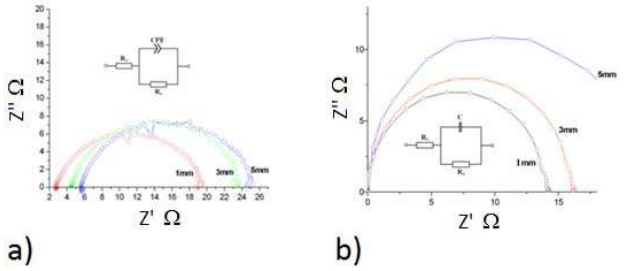

Figure 7. Real and imaginary parts of the Water electrolysis cell impedance and corresponding equalent circuits in 0.1M KOH solution (a); at three different electrode spacings in deionized water (b).

It can be shown that modeling the impedance spectrum of electrolysis cell containing 0.1M KOH solution with equivalent circuit (Figure 7a), the relaxation time of the electric double-layer capacitance and charge transfer resistance of the system is of the order of milliseconds. Performing similar analysis for impedance spectrum of electrolysis cell containing deionized water (Figure 7b), the system relaxation time is the order of microseconds, which corresponds to the geometric capacity of water electrolysis cell and the water molecule dipole orientation resistance. Since reducing the electrode spacing (increasing geometric capacity), the voltage value after fast growth falls, it can be concluded that the pulse energy is determined before the application to electrolysis cell. Naturally, the increase in capacity which drives pulses with the same energy, the voltage value on capacitor decreases.

It is known that the hydrogen release reactions on platinum and tungsten electrodes in electrolysis cell are fundamentally different. Hydrogen adsorption on the Pt surface immediately after the charge transfer reactions plays a big role in hydrogen release kinetics on platinum electrode [7]. Such adsorption does not occur on the tungsten electrode. Platinum electrode has less overvoltage comparing with tungsten electrode and both have different electrochemical potentials [7]. From measurements of voltage and current oscillograms of platinum and tungsten electrodes in electrolysis cell with two solutions in different concentration (Figure 8) shows that changing the electrodes, the voltage pulses do not change their fast growth front and slow relaxation, and increasing the solution concentration, the voltage pulse amplitude decreases with increasing current pulse amplitude for both metals. Current pulses also are similar on platinum and tungsten electrodes of the same concentration of KOH solution.

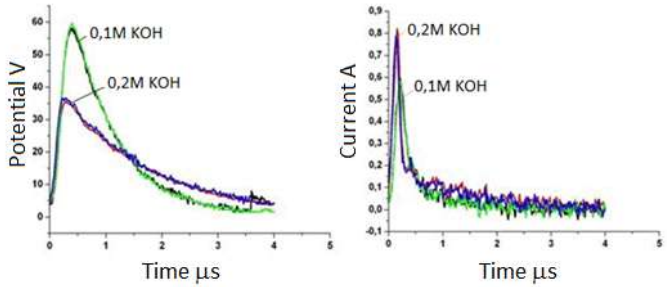

Figure 8. Voltage and current oscillograms on Pt and W electrodes (practically coincides).

Interesting results found in experiments by measuring concentration of the dissolved hydrogen with microsensor close to cathode in pulse electrolysis process, which shows that the concentration of the dissolved hydrogen on tungsten electrodes increases faster than on the platinum electrodes (Figure 9). Concentration of released hydrogen on the platinum electrode in 0.2M KOH solution starts with a smaller slope like on tungsten electrode, and after about 50 seconds the slopes of hydrogen growth on both platinum and tungsten electrodes are equal.

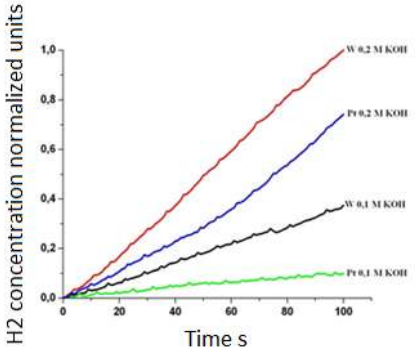

Figure 9. The nature of increase the concentration of dissolved hydrogen in the solution in close proximity to tungsten and platinum electrodes in electrolysis cell.

Platinum electrode has pronounced hydrogen adsorption area in the beginning of voltage pulse applied to electrolysis cell, what is lacking for tungsten electrode. Since the inductive voltage pulse energy is limited, and then this energy to the platinum electrode is exhausted when the adsorption process is not finished yet, and monolayer of adsorbed hydrogen is made in this process. Tungsten electrode, in its turn, has not typical hydrogen adsorption area, so the applied voltage pulse transforms in hydrogen molecule directly, which is detected by the dissolved hydrogen sensor. Approximately 50 seconds is needed when hydrogen adsorption

and desorption reaches a dynamic balance on the platinum electrode, further release of hydrogen is as effective as on the tungsten electrode.

Current-voltage characteristic for pulse electrolysis like as for direct current electrolysis mode can be found changing the amplitude of inductive voltage and calculating effective values of current and voltage pulses. Registered current and voltage oscillograms for pulses with 12 different voltage amplitudes in the cell with 0.1M KOH electrolyte and steel electrodes with spacing of 1 mm are shown in Figure 10a. The current effective values of all pulse amplitudes is calculated from measured amount of released hydrogen using gas-displacement method, and the results 12 effective values of current were obtained to construct VA plane. This procedure was repeated 0,5M and 0.3M KOH solution, at the electrode distances of 1, 3 and 5 mm.

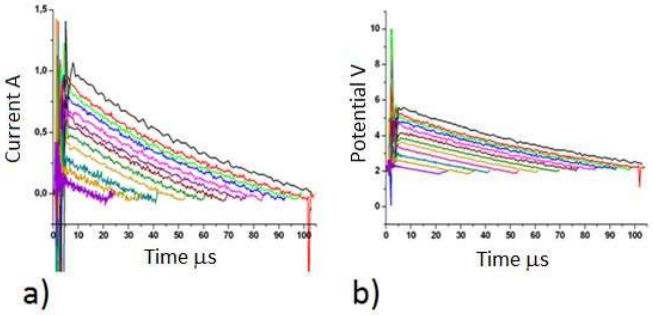

Figure 10. A current (a) and voltage (b) oscillograms of different pulse amplitudes in pulses electrolysis cell with 0.1 M KOH solution at 1 mm distance between steel electrodes.

To find the effective value of voltage taking into account the possible charge separation between cell's geometric capacitance and the electric double-layer charging with following Faraday reactions, the voltage oscillograms must be modified. To explain it, the equivalent circuit of water electrolysis cell (at the top) and interpretation of circuit's elements in molecular scale (bottom) are given in Figure 11: C_G - geometric cell capacity arising between the two electrodes and an aqueous solution as a dielectric medium; C_{EDL} - an electric double-layer capacity and R_{LP} - the charge transfer resistance; R_V - the electrolyte resistance.

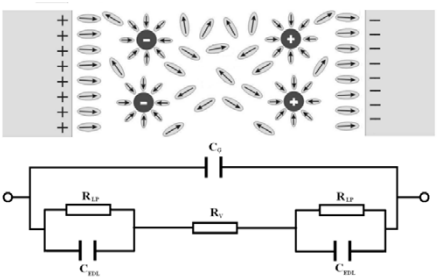

Figure 11. Location of water molecules and ions in electrolysis cell (top) and its equivalent circuit (bottom).

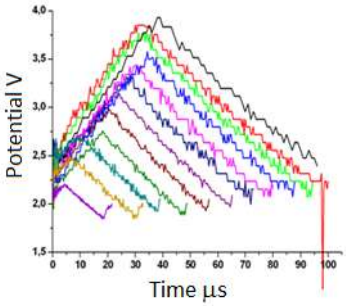

Figure 12. Modified voltage oscillograms of the electric double-layer metal/electrolyte interface.

As only cell's geometric capacity is active during fast charging period, then there is no reason to assume that immediately after the rapid pulse ending the electric double-layer capacity will be charged. On the contrary, it will keep the same potential as between pulses due to their inability to respond to the rapid changes in potential. Only cell's geometric capacity will react, which will store the energy released in fast pulse charging period. But after the end of charge stored energy in the geometric cell capacity will be reloaded to electric double-layer capacity and increase the potential on the cell. When potential on cell exceeds over-potential of hydrogen evolution, charge transfer reactions will start and gases hydrogen and oxygen releases on both electrodes. Therefore, to determine the true voltage values on C_{EDL} and R_{LP}, the voltage oscillograms should be modified as shown in Figure 12. From modified voltage pulse oscillograms effective voltage values are obtained and together with already obtained current effective values are plotted in volt-ampere curve, ready to compare with volt-ampere curve in direct current electrolysis cell (Figure 13).

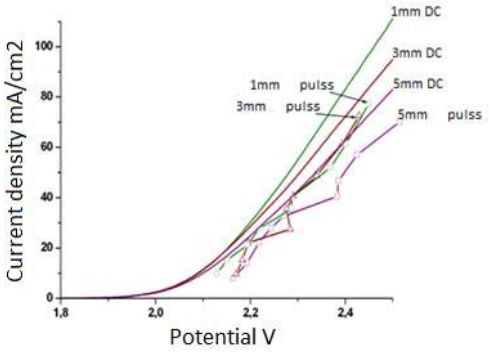

Figure 13. Volt-amperic curves of pulsed electrolysis mode (curves with points) and DC electrolysis mode (smooth curves) in the cell, which contains 0,5M KOH solution and two steel electrodes in different distances.

Comparison of volt-ampere curves shows that in the weak and also in 0.1M KOH solution pulse electrolysis is intense as the DC mode - slope is almost twice steeper. By contrast, in 0.3 and 0,5M KOH solutions the steepness of pulse electrolysis volt-ampere curve is almost the same as the DC mode. Similarity of volt-ampere curves (for example, Figure 13) for both pulse mode and DC mode approves the applicability of our empiric approach to obtain volt-ampere curve for pulse electrolysis from oscillograms to compare with DC electrolysis. This confirms discussed above hypothesis that the inductive voltage pulse in rapid growing phase is charging only geometric capacity of electrolysis cell, and only then the charging of the electric double-layer capacity and parallel starting charge transfer (electrolysis) process.

Fe_2O_3 anode for water photo-electrolysis: synthesis and properties

Comparison of electroplating and spray pyrolysis methods

Light-yellow thin films are obtained in electroplating method, suggesting the presence of iron oxyhydroxide FeOOH [8]:

$$3H_2O_2 + 2FeF^{2+} + 6e- \rightarrow 2FeOOH + 2F- + 2H_2O \qquad (A)$$

After annealing at 450 ^oC for 1h films converts to red-brown colour, suggesting the presence of hematite.

A homogeneous reddish layer without visible cracks or unsealed areas is obtained with spray pyrolysis method. After annealing these films they did not change colour, so for further investigations both annealed and as-obtained films were used.

SEM micrographs of the surface morphology of deposited thin films are shown in Figure 1. The surface of the annealed thin film obtained by ED (Figure 14 (a)) is constructed from necked nanosized grains with average diameter ~30 nm and narrow size distribution. The presence of mesopores between adjacent grains and deep cracks with a width of 20–50 nm in the entire volume of the thin film also was observed. The SEM images of the as-prepared thin film obtained by SP reveal partly amorphous structure (Figure 14 (b)) and the presence of flake-like spines with length around 100 nm and diameter of 15 nm indicating the presence of FeOOH [9]. After annealing at 450°C for 1h the SP film exhibited granular morphology where the sizes of granules were below 20 nm (Figure 14 (c)). Overall, in comparison with samples obtained by ED, the SP derived thin films are denser and consist from smaller close-packed grains.

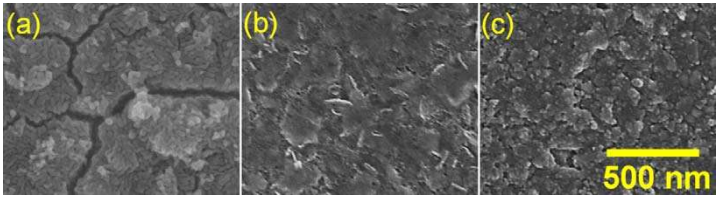

Figure 14. SEM micrographs of surfaces of thin films obtained with ED method and annealed (a), SP method as obtained (b) and SP method annealed (c).

The XRD analysis (Figure 15) revealed the formation of α-Fe_2O_3 for both ED and SP derived thin films annealed at 450°C for 1h. The hematite structure is confirmed by characteristic peaks at angles 2θ = 24, 33, 35, 41, 49, 54, 62 and 64. The XRD patterns also show strong peaks related to transparent conducting oxide FTO layer.

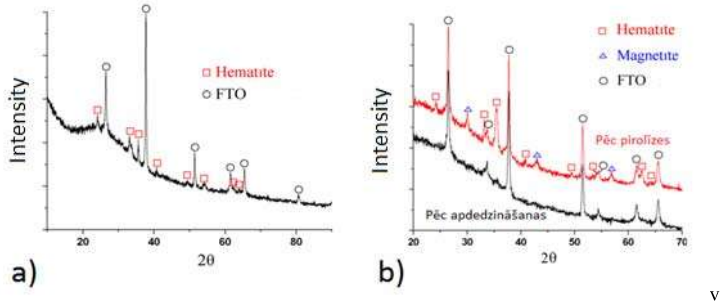

v

Figure 15. XRD spectra of thin hematite film obtained by ED method and annealed at 450 °C (a) and thin hematite films obtained with SP method before (b red) and after (b black) annealing at 600 °C.

The crystallite size of α-Fe_2O_3 was calculated from the most intense XRD peak from hematite structure at angle 2θ=35. For both samples the average crystallite size was around 15 nm.

Calculated crystallite sizes in thin films obtained by SP correlates with grain size observed from SEM image, while average crystallite size in thin film obtained by ED is smaller than that of the individual grain, indicating their polycrystalline nature.

Comparing the observed photocurrent values for α-Fe_2O_3 thin films obtained by SP and ED, it can be seen that ED derived samples has higher photocurrents for all thicknesses (Figure 16). Observed higher photocurrent values for ED films can be attributed to the presence of mesopores between adjacent grains thus increasing active reaction area and light absorption capability. It is well-known that construction of mesostructured thin films is one of the most effective strategies to enhance PEC performance [9]. Other key parameter which remarkably affects PEC performance of α-Fe_2O_3 photoanodes is thickness.

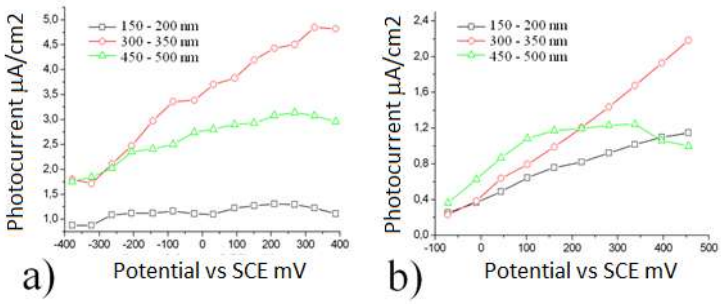

Figure 16. Results of photo-current measurements for hematite thin films with different thicknesses obtained wit ED (a) and SP (b) methods.

It has been demonstrated that by the regulation of thickness it is possible to balance photon absorption and charge carrier transport to reach higher PEC performance [10]. Due to short hole diffusion length in hematite (2-4 nm), it is necessary to decrease film thickness. However, decreasing film thickness results in the loss of light absorption. The optimal film thickness for both ED nd SP derived α-Fe_2O_3 thin films was found to be around 300nm. The highest photocurrent on the 300 nm thick porous hematite film was achieved also by Shen et all [10].

To find out flat-band potential, the concentration of the charge carriers and depletion layer width, Mott–Schottky plots were performed from the electrochemical impedance measurements where the capacitance at the photo-electrode/electrolyte junction for varying electrode potential was measured. Mott–Schottky plots obtained for ED and SP derived hematite thin films with different thicknesses are shown in Figure 17. All the thin films exhibited positive slopes, confirming the n-type conductivity for all samples. The intrinsic n-type conductivity in hematite is caused by oxygen vacancies which are compensated by reducing Fe^{3+} to Fe^{2+}. An oxygen vacancy will carry two effective positive charges, because the site will be missing two electrons compared to lattice oxygen. The overall charge neutrality of the whole lattice would then cause compensation by decreasing oxidation state of iron cations, thus offering the possibility for electron hopping: $Fe^{3+} + e^- \leftrightarrow Fe^{2+}$.

The flat-band potential, concentration of charge carriers and depletion layer width calculated from the Mott–Schottky plots are shown in Table 2. As it can be seen from Figure 17 and Table 2, by decreasing the film thickness the flat-band potential shifts to the negative (cathodic) potential side. More negative values of the flat-band potential indicate more effective separation of the photoinduced charge carriers and energy level shifting in a better position against water redox potential, thus facilitating the water photolysis reaction. In the same time, the thinnest hematite films have insufficient light absorption capacity to provide high PEC performance.

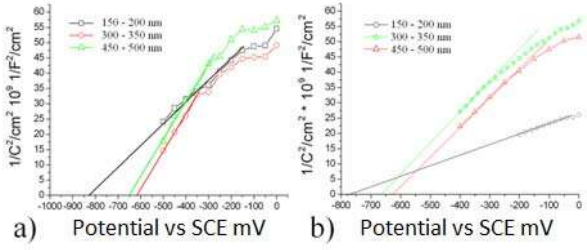

Figure 17. Mott-Schottky plots of hematite thin films obtained with ED (a) and SP (b) methods.

Table 2. Mott-Schottky analysis of ED and SP deposited hematite thin films

Thickness of thin film	**Plating mode**			**Spray pyrolysis mode**		
	E_{FB} against SCE [mV]	**N_D*10^{20} [1/cm^3]**	**ω [Å]**	**E_{FB} against SCE [mV]**	**N_D*10^{20} [1/cm^3]**	**ω [Å]**
150-200 nm	-830	18.4	25.7	-790	32	17.8
300-350 nm	-620	9.4	24.5	-665	12.1	26.3
450-500 nm	-650	9.6	26.4	-630	11.9	25.1

The intrinsic charge carrier concentration (Table 2) was found to be higher for SP derived samples, indicating higher amounts of defects, such as Fe^{2+}, originally made by oxygen vacancies. As consequence, the smaller width of the depletion layer **ω**, calculated from value of capacity C obtained from Mott–Schottky plots and the equations (5, 6), was found for SP derived thin film with highest intrinsic charge carrier concentration $\mathbf{N_D}$ (Table 2).

Properties of α-Fe_2O_3 obtained with cathodic pulsating potential plating method

The properties of α-Fe_2O_3 thin films synthesized using pulsed cathodic potential galvanization is discussed next. Table 3 collects the pulse parameters: frequency and amplitude (potential sweep limits) and unique designation used hereinafter to identify the described specific modes - cyclical potential (PC) plating and pulse potential (PP) plating. If the thin film is synthesized in cyclic potential mode, designation will begin with a cipher PC, but if synthesized in pulse potential mode – begin with PP. Next letter represents three different voltage thresholds: A from -200mV to 0, B from -400 to +200 mV and C from -600 to +200 mV. All applied voltage thresholds were experimentally determined and is measured accordingly SCE. For example, if the potential thresholds were in the range from -200 to +200 mV, layer was not formed both in pulsating and cyclic modes; while using a threshold from +200 to +800mV, the layer was unstable and peel off from the substrate. The digit at the end of the designation is meaning the frequency of pulse: 0.25 corresponds to the frequency 0.25Hz with a 50% fill factor of the pulse, and the number 1 corresponds to a frequency of 1 Hz with a fill factor of 50%. Understandably, the influence of frequency properties of synthesized hematite films has been studied only in a pulsating potential mode, while in cycling potential mode potential the scan rate 20mV/s for all samples was used.

Table 3. Designation of the samples accordingly their plating conditions.

Cyclic potential plating mode		Pulse potential plating mode		
Region of applied potential (mV)	Sample designation	Region of applied potential (mV)	Frequency (Hz)	Sample designation
-200 to 0	PCA	-200 to 0	0.25	PPA0,25
			1	PPA1
-400 to +200	PCB	-400 to +200	0.25	PPB0,25
			1	PPB1
-600 to +200	PCC	-600 to +200	0.25	PPC0,25
			1	PPC1

X-ray diffraction curves for the samples obtained in different plating modes (Figure 18), indicates only peaks from hematite and substrate crystalline phases for all samples. Using Bragg-Scherer equation the crystallite size is calculated from the most intense characteristic peak of hematite crystalline phase. From the results, it was concluded that the samples obtained by pulsating potential mode are characterized by a smaller average crystallite sizes. The reduction of crystallite size by increasing frequency can be explained with increase of plating current due desorption of hydrogen typically formed on cathode. In cyclic potential mode the current decreases during plating because of increase of concentration of adsorbed

hydrogen at the surface of cathode, consequently locking the surface. It is shown also [9-11] that the crystallite diameter is inversely proportional to the plating current.

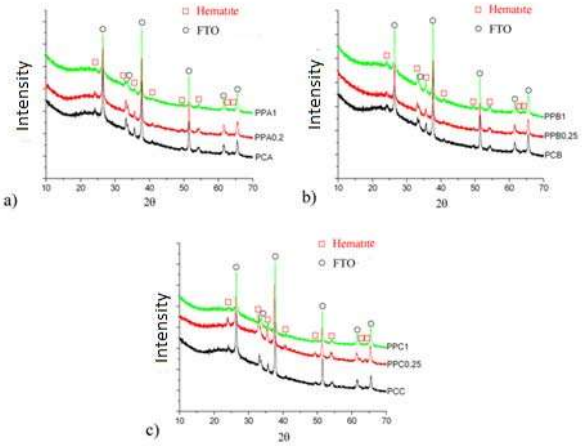

Figure 18. XRD curves for thin layer of hematite on FTO/glass substrate, obtained in cyclic and pulsating potential plating modes.

Figure 19. SEM microphotographs of hematite thin films on FTO/glass substrate, obtained in cyclic and pulsating potential plating mode.

As it is seen from SEM images (Figure 19), the surface microstructure is different for different plating modes PC and PP with two frequencies. The worm-type pellets with cracks

between them and material protrusions on the outside in the form of outward-oriented light islands are found on the surface of PCA samples. Surface of the PCB sample contains bright islands in high concentration, consisting from a cauliflower like moldings, wherein the concentration of cracks on the surface is reduced, as well as their length. Looking at the surface of PCC sample, it seems that island-type formations have exploded, leaving pores in the middle. On the surface of sample PPA0.25 does not appear pronounced grain boundaries and the gap concentration decreased significantly, indicating that the surface is homogeneous.

The character of photocurrent curves for all galvanized samples (Figure 20) is similar in all plating modes, namely the photocurrent starts from negative potential region, and is increasing up to plateau at positive potentials. Hematite thin film samples obtained in cyclic potential mode has similar photocurrent curves for all plating potential regions. The photocurrent of hematite thin film samples from A and C series obtained in PP mode at a frequency 0.25Hz is significantly higher, comparing with photocurrent for samples obtained in potential cyclic mode. Nevertheless the sample PPB0.25 has he same photocurrent as the sample PCB, which can be explained by the film microstructure (it accounts for large nanoparticle aggregates >2μm in relatively large distances >500nm each from other). This microstructure could hinder effective splitting and transfer of photo-generated charge carriers (holes), because their diffusion path length is up to 2-4 nm [12]. Similarly, the volume made from such nanoparticles aggregates has limited penetration possibility for the electrolyte and exchanged of the reaction products.

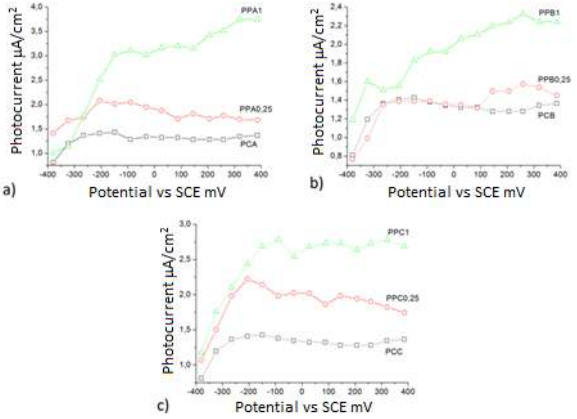

Figure 20. Characteristic photocurrent dependence for hematite thin films, obtained in different cycling and pulsating potential modes.

A series of samples obtained by changing the potential from -200 to 0 mV has the highest correlation in characteristics between physical and photo-electrochemical properties, depending on parameters of the plating process. Using cyclic or pulsating pulse potential modes as well as changing the pulsating frequency, the sizes of hematite crystallites decreases

and surface morphology changes significantly. The surface of such samples is characterized with meso-porous structure having pore sizes from 10 to 20nm. For the samples with increased photocurrent, the flat band potential shift to the negative direction, decreases concentration of basic (darkness) charge carriers and increases the barrier layer thickness. The decrease of concentration of darkness charge carriers is explained with changes in structure and composition – the concentration of oxygen vacancies in hematite is decreased, accordingly increases thickness of barrier layer [13].

Properties of α-FeO_3 thin films obtained in anodic DC plating method

The plating of anodic α-Fe_2O_3 thin films was carried out in aqueous solution 0,02M $FeCl_2$ using constant potential (1,2V) mode and voltage pulse mode with unipolar rectangular pulses with amplitude 1.2V and frequencies 0.25Hz, 1Hz and 10Hz. After synthesis film was annealed in the atmosphere of air at 450 °C during 1 hour. Constant potential mode hereinafter is described with DC.

Comparing with cathodic plating, discussed above, where the solubility of Fe^{3+} on he substrate was achieved with reduction of H_2O_2 to OH^- ions and local increase in the pH near the electrode, in anodic both pulse and DC modes the oxidation degree of iron ion is changed during plating process, where Fe^{2+} ions at the anode are returning the electrons and becoming the Fe^{3+} with limited solubility, thereby precipitates on the anode surface in the form of iron oxy-hydrate.

Influence of frequency in anodic pulse plating mode on the physical and photo-electrochemical properties of thin films were not as significant as it was observed in the case of cathodic pulse plating mode.

In turn, with anodic galvanization method using innovative improvements, the hematite thin films with increased photo-activity were obtained. It can be described next - immediately after the anodic plating of thin film in 0,02M $FeCl_2$ aqueous solution, a negative potential (-1,2V accordingly to platinum counter/reference electrode) is applied to sample, thereby reducing plated layer. It is known that the addition of a negative potential may contribute to reduction of iron oxyhydroxide ate FeOOH and formation of FeO [14] accordingly reaction: $FeOOH + e^- \rightarrow FeO + OH^-$. After synthesis the film was annealed in the atmosphere of air at 450 °C during 1 hour.

Reduced resolution SEM`s images from the surface of sintered layer (Figure 21a) shows homogeneous regions separated by cracks of various sizes. From higher resolution image it can be seen that nanostructure of thin film is complex and contains deep cracks with walls decorated with smaller particles of different shapes and average size of 25nm. XRD spectra of both un-reduced and reduced layers after annealing (Figure 21b) indicate significant differences between both films – the amplitudes of characteristic α-Fe_2O_3 peaks are decreased for reduced thin film and new lines appear, indicating the presence of FeO(OH) presence. Mean size of crystallites in reduced and annealed thin film, which calculated for the peak at $2\theta = 36$deg, is 41nm, - approximately 20nm less than for non-reduced and annealed films.

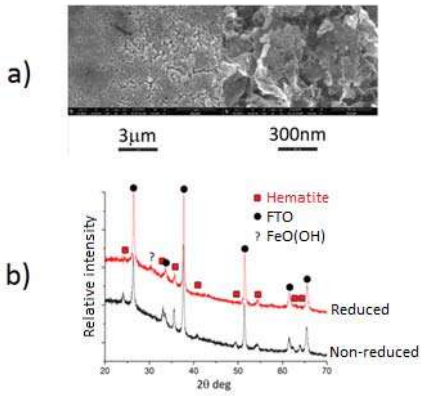

Figure 21. (a) Surface morphology of thin film obtained in anodic galvanization's reduction mode after annealing in air; (b) XRD spectra of anodic electroplated non-reduced and anodic electroplated reduced thin films after annealing in air.

The photocurrent in dependence from applied potential of both reduced and non-reduced annealed thin films (Figure 22 (a) and (b)) increases in anodic direction, pointing to the n-type conductivity of samples. The photocurrent in the region of negative potentials is higher for non-reduced thin film sample, while for reduced sample the photocurrent appears at -175mV and grows very fast at positive potentials above 200mV. At potential 400mV the value of photocurrent for reduced thin film sample is seven times higher as for non-reduced sample.

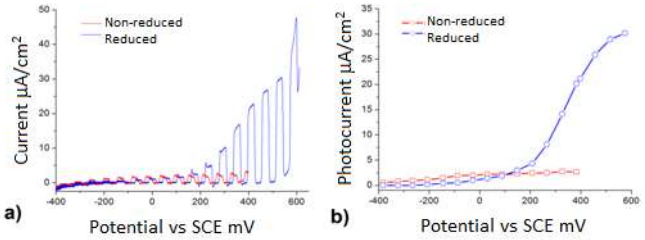

Figure 22. (a) Current-voltage characteristics of reduced and non-reduced thin film samples in the presence of chopped light; (b) the photocurrent values in dependence from potential.

To explain high photo-activity of the reduced thin film sample at anodic potentials, the light-generated photocurrent pulses at voltage range 260-360 mV of reduced and non-reduced samples are analyzed in details (Figure 23). The photocurrent of non-reduced thin film after light activation increase with some delay and reaches the maximal value, then is descending until a saturation value. The photocurrent of reduced thin film increases very fast after light activation, reaching defined value, and than increase slowly without saturation.

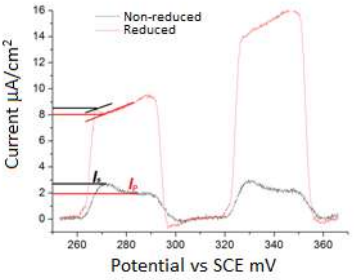

Figure 23. Assessment of the recombination degree for light-induced charge carriers in reduced and non-reduced hematite thin films.

It is known that a decrease of photocurrent when light is on can be associated with recombination of light-induced charge carriers [15]. The degree of recombination can be evaluated as relationship between the value of saturation current and the initial maximal value, $r = (1-I_p/I_s) * 100\%$. It is obtained by calculations that recombination degree for non-reduced thin film sample at 260 mV is about 30%, while only 5% for reduced thin film sample. Whereas at 325mV the calculations of recombination degree for non-reduced thin film sample gives same 30%, while value 0% is obtained for reduced thin film sample. It does not mean that in reduced thin film does not exist recombination of light-induced charge carriers. This assessment shows the limiting step in light induced photocurrent process is recombination of induced charge carriers at non-reduced hematite thin film, and recombination of basic charge carriers at reduced hematite thin film. From this point, we can conclude that the reduced thin film material has improved charge transfer characteristics, which could be the main reason for the increased photocurrent in the region of positive potentials.

The fact, why photocurrent appears to more positive potentials for reduced thin film sample comparing with non-reduced, is well explained through Mott - Schottky curve (Figure 24).

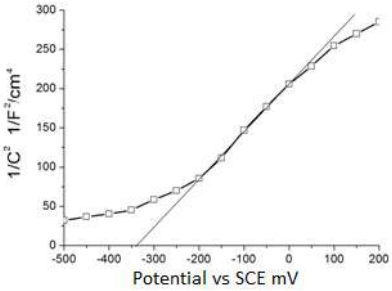

Figure 24. The Mott – Schottky plot for reduced hematite thin film sample.

As it is seen from Mott-Schottky plot, the value of flat band potential for reduced hematite thin film sample is -341mV versus SCE, and it is shifted by 359 mV to positive potential direction compared to non-reduced hematite thin film sample both obtained in anodic DC plating mode. So, the higher polarization potential must be applied to reduced hematite thin film anode, to initiate the photocurrent; and it confirms the impact of a flat band potential value on properties of charge carriers and electronic band structure on photo-electrode material. From Mott-Schottky plot it is calculated that for reduced hematite thin film sample concentration of basic (darkness) charge-carriers is $N_D = 1{,}82*10^{20}$ and barrier layer thickness at 0V potential - 5nm.

Yttrium impurity effect on α-Fe_2O_3 properties

In our work the photo-electrochemical properties of yttrium doped hematite thin films is reported. Yttrium is BIII group element with electron configuration $4d^15s^2$ and oxidation state 3^+. To the author's best knowledge, no similar studies have been explored so far. The aim of the present investigation is to find out the influence of yttrium on structure and photoelectric properties of hematite. The detailed Mott-Schottky analysis were carried out to find out flat-band potential, concentration of charge carries and the barrier layer thickness in dependence from yttrium concentration in photo-electrochemical cell.

Figure 25a shows X-ray diffraction patterns of the pure and Y doped iron oxide thin films. From these patterns it is clear that all of the synthesized films have a single phase of α-Fe_2O_3 (JCPDS file no. 86-0550). With increasing the concentration of yttrium the most intensive hematite peak from (104) plane (2θ ~ 35.5 deg.) is shifted to smaller angles (Figure 25b). Similar behavior was found previously for Al-doped hematite due to change of volume of Al-unit cell [20-24]. The expanding or shrinking of unit cell is well known effect found for number of impurities introduced into hematite and is attributed to different ionic size. Smaller cations such as Al^{3+} for example reduces the volume of unit cell and shift main XRD peaks to higher values [20] but larger cations expands unit cell and shifts XRD peaks to lower values [21-24]. Since the ion radius of Y^{3+} (104 pm) is larger than the ion radius of Fe^{3+} (69 pm), it is expected that the unit cell of hematite structure will be expanded which is in accordance with XRD results were characteristic hematite peak shifts to smaller angles.

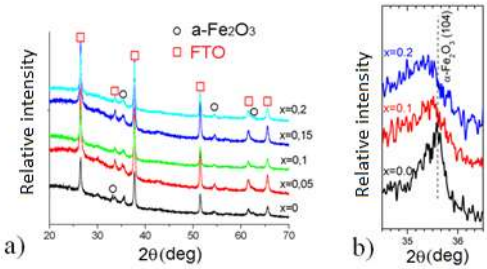

Figure 25. (a) XRD spectra of α-$Fe_{2-x}Y_xO_3$ thin films; b) detailed diffraction peak where shown how peak is shifted to lower angles if Y concentration increases.

Using the Scherrer equation, the crystallite sizes were calculated from hematite (104) peak. It was found that crystallite sizes decreases with increasing yttrium concentration. Un-doped hematite has crystallites with average size 37 nm while doped hematite (α-$Fe_{2-x}Y_xO_3$) with yttrium concentration x = 0.1 has crystallites with average size of 31 nm and for x = 0.2 the average crystallite size was 24 nm. Decreasing dimensions of crystallite sizes increase the content of the grain boundaries in the volume of photoanode what would further increase the charge transfer at interface electrode/electrolyte and the photo-current.

The XPS were used for investigating the chemical state and the electronic structure of the Y doped iron oxide thin films. Figure 3 a) displays measured Fe 2p photoelectron spectra. Spectra of undoped Y doped iron oxide thin films appear because of the spin-orbit splitting of two bands, $2p^{3/2}$ (710.8 eV) and $2p^{1/2}$ (724.7 eV), and a weak charge transfer satellite (719.2 – 719.4 eV) related to Fe^{3+} in structure. XPS analysis reveals that iron in the films is in Fe^{3+} oxidation state, forming besides Fe_2O_3, $Fe(OH)_3$ and $FeO(OH)_2$ like species (appearance of shoulder at 531.3 eV, besides main photoelectron peak at 529.7 eV in O1s spectra was observed). It was observed that Y doping did not lead to formation of Fe^{2+} species. Figure 26b shows measured Y 3d photoelectron spectra. Y 3d photoelectron band contain two components, $3d^{5/2}$ (157.3 eV) and $3d^{3/2}$ (159.4 eV), due to spin-orbit splitting. Y $3d^{5/2}$ chemical shift from 156 eV to 157.3 eV indicates that Y is not in metallic form in the sample [24], it is in 3^+ oxidation state. However in pure Y_2O_3 Y $3d^{5/2}$ photoelectron peak positions at 156.8 eV [25]. In the yttrium doped hematite films slightly higher chemical shift was observed. This shift can be related to Y in hematite lattice. Previously it is reported that Y $3d^{5/2}$ has been positioned at 157.5 eV in yttrium ortho-ferrite ($YFeO_3$) [26]. It is also demonstrated earlier that carbonates and hydroxyl-carbonate species produce positive chemical shifts in the Y binding energy [25]. However in presence of carbonate and hydroxycarbonate species the position of Y $3d^{5/2}$ is at 158.6 eV. To investigate relative yttrium concentration on sample surface, the ratios of Fe 2p and Y 3d XPS spectral band areas were used. First the Shirley background was removed using the CasaXPS software and consecutively the band areas were measured. The ratio of the Fe 2p and Y 3d was 6.6 in case of sample $Fe_{1.9}Y_{0.1}O_3$ and 3.1 in case of sample $Fe_{1.8}Y_{0.2}O_3$, indication formation of yttrium richer surface when dopant concentration in the sample was increased.

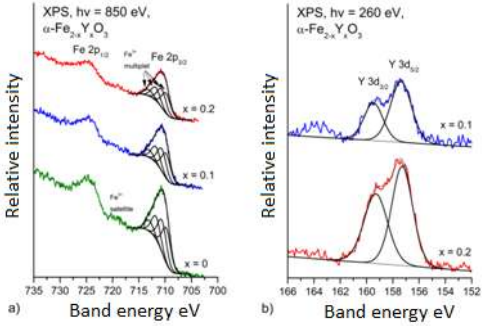

Figure 26. Photoelectron spectra of Fe 2p (a) Y 3d (b) bands of Y-doped hematite samples.

Optical properties of un-doped and doped hematite thin films on glass substrate were studied by using UV–VIS spectrophotometer. The absorbance was measured by subtracting the absorbance of the glass substrate, which was taken as a reference in all measurements. As expected all un-doped and doped hematite samples exhibit intensive absorption in a wide wavelength range from UV to visible light. Suitable band gap energy for visible light absorption in hematite is due to indirect Fe d-d transitions between split in the ligand field Fe 3d orbitals. The indirect optical band gap energy of the thin films was calculated from plot $(\alpha h\nu)^{1/2}$ vs hν (eV) where α is the absorption coefficient, but hν is the photon energy in eV. To calculate the value of the indirect optical band gap energy of the films the plot were extrapolated from the intercept of the straight line from the graphs. The calculated indirect optical band gap energy for un-doped hematite is 1.84 eV while for yttrium doped hematite samples they are decreasing to 1.75 eV ($Fe_{1.9}Y_{0.1}O_3$) and 1.7 eV ($Fe_{1.8}Y_{0.2}O_3$).

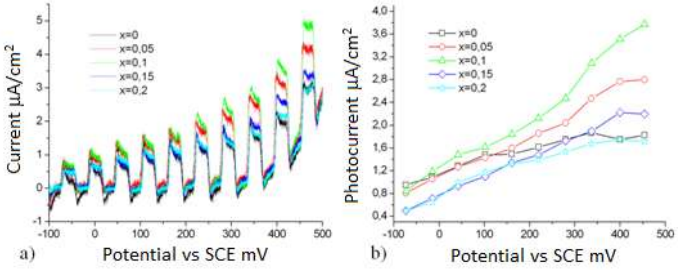

Figure 27. Photo-electrochemical performance of un-doped and yttrium doped hematite thin films $Y_xFe_{2-x}O_3$, were x = 0; 0.05; 0.1; 0.15; 0.2: a) light-chopped current–potential plots and b) photocurrent–potential curve.

Measurements of volt-ampere curve with pulsating light source indicate the increase of photocurrent in anodic direction, what confirms n-type conductivity (Figure 5a) for all synthesized un-doped and yttrium doped hematite thin films. Photoelectrochemical performance of thin films is higher when Fe^{3+} is substituted by Y^{3+} in hematite lattice. The photocurrent attained maximum when yttrium concentration was x=0.1 ($Y_xFe_{2-x}O_3$), thus it seems that it is the optimal concentration above which the observed photocurrent density decreases. The decrease in the photocurrent beyond certain doping level could be attributed to the fact, that higher concentration of dopant would provide more defect-scattering/recombination properties [10].

Measurements of volt-ampere curve with pulsating light source indicate the increase of photocurrent in anodic direction, what confirms n-type conductivity (Figure 5a) for all synthesized un-doped and yttrium doped hematite thin films. Photoelectrochemical performance of thin films is higher when Fe^{3+} is substituted by Y^{3+} in hematite lattice. The photocurrent attained maximum when yttrium concentration was x=0.1 ($Y_xFe_{2-x}O_3$), thus it

seems that it is the optimal concentration above which the observed photocurrent density decreases. The decrease in the photocurrent beyond certain doping level could be attributed to the fact, that higher concentration of dopant would provide more defect-scattering/recombination properties [10].

To understand the charge transport within the un-doped and yttrium doped hematite thin films, as well as to find out flat band potential, concentration of charge carriers and depletion layer width, the Mott-Schottky measurements were performed where the capacitance at photoelectrode/electrolyte junction for varying electrode potential was measured. Mott-Schottky plots obtained for un-doped and yttrium doped hematite thin films are shown in Fig. 28. All the thin films exhibited positive slopes, confirming the n-type conductivity for all samples. The flat band potential, concentration of charge carriers and depletion layer width calculated from the Mott-Schottky plots are shown in Table 1.

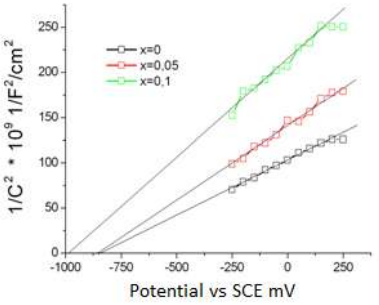

Figure 28. Mott-Schottky plots for different $Y_xFe_{2-x}O_3$ samples (Mott-Schottky plots for are not shown here for samples x=0.15 and 0.2 due to the different dimensions).

Table 4. Data compiled from Mott-Schottky plots – flat band potential (E_{FB}), intrinsic charge carrier concentration (N_D), depletion layer width (ω).

$Y_xFe_{2-x}O_3$	E_{FB} vs SCE [mV]	N_D *10^{20} [1/cm^3]	ω [Å]
x=0	-814	9.69	11
x=0.05	-833	6.67	16
x=0.1	-962	5.71	23
x=0.15	-1061	2.70	58
x=0.2	-1171	2.06	78

As it is seen from Table 4, with increasing the concentration of yttrium doping in hematite the flat band potential shifts to the negative (cathodic) potential side from -814 mV versusSCE

(Fe_2O_3) to -1171 mV versus SCE ($Y_{0.2}Fe_{1.8}O_3$). More negative value of the f atband potential indicates more effective separation of photoinduced charge carriers and energy level shifting in a better position against water red-ox potential thus facilitating the water photolysis reaction. The intrinsic charge carrier concentration was also found to decrease (Table 4) indicating smaller amount of defects such as Fe^{2+} originally made by oxygen vacancies. As consequence of decreased intrinsic charge carrier concentration width of depletion layer increases (Table 4) which results in partial depletion of electrons from the film. Overall, the shift of flat band potential and increase of depletion layer width facilitate separation of photo-induced charge carriers [5], which is the key factor for successful water splitting.

In summary, yttrium doped hematite thin films ($Y_xFe_{2-x}O_3$) were deposited successfully by spray pyrolysis method using aqueous solutions of metal chlorides. SEM studies revealed that all thin film samples completely covers the substrate and layers have closely packed grain structure, flat surface and thickness below 500 nm. XRD measurements shown single phase hematite formation, but XPS studies confirmed yttrium incorporation into hematite lattice. Photo-electrochemical performance of hematite thin films increased by substituting Fe^{3+} with Y^{3+} in hematite lattice. The photocurrent attained maximum when yttrium concentration was x=0.1 ($Y_xFe_{2-x}O_3$). Detailed analysis of Mott-Schottky plots shown, that increase of yttrium concentration shifts the flat-band potential to cathodic direction, the concentration of intrinsic charge carriers decreases and the width of depletion layer increases, thus increasing the concentration of long-living separated photo-induced charge carriers and has positive impact on the photo-electrochemical performance.

Overall conclusions

1. Water electrolysis with inductive voltage pulses:

1.1. Inductive voltage pulse when applied to the water electrolysis cell is divided into two significantly different sections: fast charging at the beginning (in the first microsecond) and slow discharge below (long and flat tail);

1.2. Quick charge is related to charge of the electrolysis cell geometric capacitance (smaller capacity in cell's equivalent scheme), but long discharge tail reflects transfer of the accumulated in geometric capacitor electric charge to the double-layer capacitor and it discharge through charge transfer reactions on the interface electrolyte/metal;

1.3. Kinetics of inductive voltage and current pulses in water and weak electrolyte does not differ on tungsten and platinum electrodes, although hydrogen evolution reactions on these two materials substantially differ;

1.4. It is determined with the microelectrode sensor that the concentration of dissolved hydrogen near to the platinum electrode grows more slowly than near to the tungsten electrode, when inductive voltage pulse electrolysis proceeds; this difference decreases with increasing electrolyte conductivity. The difference is explained by the formation of a layer of adsorbed hydrogen on the platinum electrode at the beginning of electrolysis process.

1.5. An empirical method was developed to compare volt-ampere characteristics for pulse and DC electrolysis using average value approximation for current and voltage pulses.

2. Development of methods to synthesize ion oxide electrodes for water photolysis and research of properties of obtained thin film electrodes:

2.1. Mixed composition (hematite + magnetite) poorly structured (flake-type morphology) thin films with medium photo-activity is obtained with spray pyrolysis method;

2.2. High purity nanostructured (granular morphology) hematite α-Fe_2O_3 thin films are obtained with cathodic plating method in linearly cycling potential mode, and characterize with three times higher photocurrent comparing to spray pyrolysis method; advantages of the photo-electrode obtained in cathodic galvanization process are phase purity and pronounced surface nanostructures;

2.3. High-purity α-Fe_2O_3 nanostructured thin films are obtained with cathodic plating method in pulsed potential mode, for which the photocurrent is greater comparing with thin films produced in the linear cycling potential mode; wherein photocurrent increases with growing the frequency of the plating pulses;

2.4. Varying the width of rectangular cathodic voltage pulses from 0mV to -200mV the average crystallite sizes in galvanized hematite thin films decreases; the microstructure of surface becomes more homogeneous with increasing frequency;

2.5. By increasing the pulse frequency in anodic plating method, thin hematite films are obtained for which the flat band potential shifts to cathodic direction, that facilitates water ox-

red reaction progress in the light, wherein concentration of basic charge carriers decreases and thickness of the barrier layer formed on the boundary electrode-electrolyte increases;

2.6. It is found that after the anodic plating of iron oxy-hydroxide thin film, by providing negative potential to it in a same solution, the FeOOH is reduced to FeO, and after annealing at 450 °C air atmosphere for 1h it transforms into pure hematite phase; thereby providing a material with seven times higher photocurrent than a typically obtained in anodic plating;

2.7. Flat band potential is depending on film thickness, - it is found that for the thinner films flat band potential is shifted towards negative potentials (cathodic direction); thinner films have higher concentration of basic charge carriers.

2.8. For the first time the Yttrium doped iron oxide thin films are synthesized with spray pyrolysis method, the XRD spectra confirms the presence of only hematite phase, wherein the increasing the concentration of yttrium, increases the volume of hematite elementary cell and decreases the average size of crystallites;

2.9. Y^{3+} ion in the hematite structure replaces Fe^{3+} ion in oxygen octahedron, reduces the oxygen vacancy concentration and accordingly the concentration of basic (darkness) charge carriers, increases the barrier layer thickness, shifts flat band potential to cathodic direction and enhance separation of photo-excited charge carriers (electron-hole pairs);

2.10. Photocurrent has the maximum value at a concentration 0.1 of yttrium in doped hematite $Y_{0,1}Fe_{1,9}O_3$; that is more than two times higher as in pure hematite; by increasing yttrium concentration above 0.1 ($Y_{0,1}Fe_{1,9}O_3$) the impurity elements begin to act as recombination centers and decrease photo-activity.

THESES TO BE DEFENDED

1. Specific surface area and porosity of hematite (a-Fe_2O_3) photo-electrolysis anode can be improved, if before the final annealing the originally obtained iron oxy-hydroxide (FeOOH) thin films are cathodically polarized in the precursor solution, because the film is reduced to the products which during final crystallization forms pure hematite phase with the desired morphology.

2. The photo-activity of Yttrium doped (up to a certain concentrations) hematite (α-Fe_2O_3) photo-anode thin film increases due to the impurity Y^{3+} ion entry in place of Fe^{3+} ion shifting the flat band potential to cathodic direction.

3. With short voltage pulses applied to water electrolysis cell in weak electrolytes next processes can be separated: firstly the capacitor of a water electrolysis cell is charged, than this charge is moved to the electric double-layer and charge transfer reaction (electrolysis) processes.

REFERENCES

1. Ghoroghchian J., Bockris J. O'M. Use of a Homopolar Generator in Hydrogen Production from Water// International Journal of Hydrogen energy. – 1985. – Nr.2. – 10
2. Vanags M., Kleperis J. and Bajars G. (2012) Water Electrolysis with Inductive Voltage Pulses. Chapter 2 in Book: Electrolysis, Editors Janis Kleperis and Vladimir Linkov, InTech (2012), pp.19-44, doi.org/10.5772/52453
3. Shimizu N., Hotta S., Sekiya T., Oda O. A novel method of hydrogen generation by water electrolysis using an ultra-short-pulse power supply// Journal of Applied Electrochemistry – 2006. – Nr.36. – 419. – 423.lpp.
4. Mazloomi K., Sulaiman N., Moayedi H. An Investigation into the Electrical Impedance of Water Electrolysis Cell – With a View to Saving Energy// International Journal of Electrochemical Science. – 2012. – Nr.7. – 3466. – 3481.lpp.
5. Gan L. M., Bakar R. A., Chang S. L. Development of Multi Duty Cycle Sequential Gated Pulse Frequency Generator for Resonant Electrolysis// ISBN: 987-967-5080-9501
6. Popov K. I., Keča D. N., Vidojkovič S. I. Mathematical model snd digital simulation of pulsating overpotential copper electrodeposition// Journal of Applied Electrochemistry – 1976. – Nr.6. – 365. – 370.lpp.
7. Tomar M.S., Garcia F.J. Spray pyrolysis in solar cells and gas sensors// Progress in Crystal Growth and Characterization – 1981. – Nr. 4. – 221. – 248. lpp.
8. Macdonald R. J. Comparison and discussion of some theories of the equilibrium electrical double layer in liquid electrolytes// Journal of Electroanalytical Chemistry – 1987. – Nr.223. – 1. – 23.lpp
9. Richardo Schrebler et al "An Electrodeposition Route for Obtaining a-Fe2O3 Thin Films", Electrochem and Solid State Letters, 9 (7) C110-C113 (2006)
10. Qua N. S., Zhua D., Chanb K. C., Leia W.N. Pulse electrodeposition of nanocrystalline nickel using ultra narrow pulse width and high peak current density// Surface and Coatings Technology – 2003. – Nr168. – 123. – 128.lpp.
11. Pavlatou E. A., Raptakis M., Spyrellis N. Synergistic effect of 2-butyne-1,4-diol and pulse plating on the structure and properties of nickel nanoctystalline deposits// Surface and Coatings Technology – 2007. – Nr.201. – 4571. – 4577.lpp.
12. Paunovic M., Schlesinger M. Fundamentals of Electrochemical Deposition// Electrochemical Society Series – 1998.
13. Barroso M., Pendlebury S. R., Cowan A J., Durrant J. R. Charge carrier trapping, recombination and transfer in hematite (α-Fe2O3) water splitting photoanodes// Chemical Science – 2013. – Nr.4. – 2724.
14. Armelao L., Bettinelli M., Casarin M., Granozzi G., Tondelloy E., Vittadini A. A theoretical and experimental investigation of the electronic structure of α-Fe2O3 thin films// Journal of Physics: Condensed Matter – 1995. – Nr.7. – L299. – L305.lpp.
15. Nomura K., Ujihira Y. Conversion Electron Mijssbauer Study of Thin Film Iron Oxide Photoelectrodes// Thin Solid Films – 1985. – Nr.I28. – 225. – 230.lpp.
16. Schrebler R. S., Bello K., Vera F. Cury P., Muñoz E., del Río R., Meier H. G., Córdova R., Dalchiele E. A. The influence of different electrodeposition E/t programs

on the photoelectrochemical properties of α-Fe2O3 thin films// Thin Solid Films – 2010. – Nr.518 – 6844. – 6852.lpp.
17. NIST Chemistry WebBook// http://webbook.nist.gov/chemistry/
18. Yu Q., Fu W., Yu C., Yang H., Wei R., Sui Y., Liu S., Liu Z., Li M., Wang G., Shao C., Liu Y., Zou G. Structural, electrical and optical properties of yttrium-doped ZnO thin films prepared by sol–gel method// Journal of Physics D: Applied Physics – 2007. – Nr.18. – 40. – 5592. – 5597.lpp.
19. Yu Q, Yang H., Fu W., Chang L., Xu J., Yu C., Wei R., Du K., Zhu H., Li M., Zou G. Transparent conducting yttrium-doped ZnO thin films deposited by sol–gel method// Thin Solid Films – 2007. – Nr.7-8. – 515. – 3840. – 3843.lpp.
20. Kleiman-Shwarsctein A., Huda M. N., Walsh A., Yan Y., Stucky G. D., Hu Y-S., Al-Jassim M. M., McFarland E. W. Electrodeposited Aluminum-Doped α-Fe2O3 Photoelectrodes: Experiment and Theory// Chemistry of Materials – 2010. – Nr.22. – 510. – 517.lpp.
21. Rivera R., Pinto H. P., Stashans A., Piedra L. Density functional theory study of Al-doped hematite// Physica Scripta – 2012. – Nr.85. – 015602.
22. Zachary D., Pozun, Henkelman G. Hybrid density functional theory band structure engineering in hematite// The Journal of Chemical Physics – 2011. – Nr.134. – 224706.
23. Wagner C. D., Riggs W. M., Davis L. E., Moulder J. F. Handbook of X-Ray Photoelectron Spectroscopy// Perkin-Elmer Corp – Physical, Electronics Division: Eden Prairie – MN – 1979.
24. Gougousi T., Chen Z. Deposition of yttrium oxide thin films in supercritical carbon dioxide// Thin Solid Films – 2008. – Nr.516. – 6197. – 6204.lpp.
25. Racu A.V., Ursu D.H., Kuliukova O.V., Logofatu C., Leca A., Miclau M. Direct low temperature hydrothermal synthesis of YFeO3 microcrystals// Materials Letters – 2015. – Nr.140. – 107. – 110.lpp.
26. Kumari S., Singh A. P., Tripathi C., Chauhan D., Dass S., Shrivastav R., Gupta V., Sreenivas K., Satsangi V. R. Enhanced Photoelectrochemical Response of Zn-Dotted Hematite// International Journal of Photoenergy – 2007. – Article ID 87467 – 6 pages.

AUTHOR'S PUBLICATIONS

Articles in journals and collections of scientific articles

Articles in peer-reviewed journals (there are SCOPUS):

1. M. Vanags, J. Kleperis, G. Bajars, A. Lusis, Water electrolysis using electrodes with modified surface/volume **(2007) Journal of Physics: Conference Series** 93 (2007) 012025. DOCUMENT TYPE: Conference paper; SOURCE: Scopus

2. Martins Vanags, Janis Kleperis and Gunars Bajars, Electrolyses model development for metal/electrolyte interface: Testing with micro-respiration sensors **(2011) International**

Journal of Hydrogen Energy, Volume 36, Issue 1, January 2011, Pages 1316-1320. DOCUMENT TYPE: Conference paper; SOURCE: Scopus

3. M. Vanags, J. Kleperis and G. Bajars. Separation of Charging and Charge Transition Currents with Inductive Voltage Pulses **(2011) Latvian Journal of Physics and Technical Sciences**, Volume 48, Number 3 / 2011, p. 34-40. DOCUMENT TYPE: Article; SOURCE: Scopus

4. Aizpurietis, P., Vanags, M., Kleperis, J., Bajars, G. Ni-al protective coating of steel electrodes in dc electrolysis for hydrogen production **(2013) Latvian Journal of Physics and Technical Sciences**, 50 (2), pp. 53-59. DOCUMENT TYPE: Article; SOURCE: Scopus

5. Liepina, I., Bajars, G., Lusis, A., Mezinskis, G., Vanags, M. Preparation and characterization of nanostructured Fe-TiO2 thin films produced by electrophoretic deposition **(2013) IOP Conference Series: Materials Science and Engineering,** 49 (1), art. no. 012060, DOCUMENT TYPE: Conference Paper; SOURCE: Scopus

6. Vanags, M., Kleperis, J., Bajars, G., Nemcevs, V. Electrodeposition of Nanoporous Nickel Layers Using Inductive Voltage Pulses. **(2013) IOP Conference Series: Materials Science and Engineering**, 49 (1), art. no. 012008, . DOCUMENT TYPE: Conference Paper; SOURCE: Scopus

7. Andris Šutka, Martins Millers, Nicola Döbelin, Rainer Pärna, Martins Vanags, Mihael Maiorov, Janis Kleperis, Tanel Käämbre, Urmas Joost, Ergo Nõmmiste, Vambola Kisand and Maris Knite. Photocatalytic activity of anatase–nickel ferrite heterostructures **(2015) Physica status solidi (a)**, 20 Jan 2015; DOI: 10.1002/pssa.201431681

8. Andris Šutka, Martins Millers, Martins Vanags, Urmas Joost, Mihael Maiorov, Vambola Kisand, Rainer Pärna, Inna Juhnevica. Comparison of photocatalytic activity for different co-precipitated spinel ferrites **(2015) Research on Chemical Intermediates**, 4 March 2015; DOI: 10.1007/s11164-015-1969-6

9. Martins Vanags, Andris Šutka, Janis Kleperis, Peteris Shipkovs. Comparison of the Electrochemical Properties of Hematite Thin Films Prepared by Spray Pyrolysis and Electrodeposition **(2015) International Ceramics**, 13 Jan 2015; DOI:10.1016/j.ceramint.2015.03.272

10. Martins Vanags, Andris Šutka, Janis Kleperis, Arturs Medvids, Pavels Onufrijevs, Janis Klavins, Rainer Pärna, Vambola Kisand. Yttrium Doped Hematite Nano-Grain Thin Films as Anode Material for Solar Water Splitting **(2015) Thin Solid Films**, submitted for publication

Articles in other journals:

1. Ķīsis G., Zeps M., Vanags M. Parameters of an efficient electrolysis cell **(2009) Latvian Journal of Physics and Technical Sciences. Riga, 2009, N3. 6** p. Nav Scopus

2. Martins Vanags, Peteris Shipkovs, Janis Kleperis, Gunars Bajars, Andrejs Lusis. Water Electrolyses – Unconventional Aspects **(2009) In Book: "Selected Articles Of Hydrogen Phenomena** "As the Memory of IHEC 2007 on the Occassion of UHK **2009**" Editors: T. Nejat Vezġroğlu, M. Oktay Alniak, Ġenay Yalçin; 1.Basım: Ekim 2009, ISBN: 978-605-5936-23-5, p. 39-45.

4. Vanags M., Aizpurietis P., Bajars G., Kleperis J., Klavins J. Water electrolysis with DC pulses and plasma discharge **(2012) International Scientific Journal for Alternative Energy and Ecology ISJAEE, No 9 (113) 2012**, pp.21-27 (nav SCOPUS)

5. Vanags M., Kleperis J. and Bajars G. **(2012)** Water Electrolysis with Inductive Voltage Pulses. **Chapter 2 in Book: Electrolysis, Editors Janis Kleperis and Vladimir Linkov, InTech (2012)**, pp.19-44, doi.org/10.5772/52453

Patents

1. M. Vanags, V.Ņemcevs, J.Kleperis, Water-powered combined heat and power supply system. Latvian patent LV 13710, 2007 Published: "Patents and Trademarks", 5 / In 2008., Lpp.679.

2. P. Liopa, M. Vanags. Ion generator combustion engine and boiler operating efficiency. Latvian patent LV 14416 B; publ. 2012 (application: Nr. P-10-49, 23.03.2010).

Conference abstracts

2014.g.
The 30th Scientific Conference of Institute of Solid State Physics, University of Latvia, February 19 – 21, 2014, Riga (Latvia)
1. S-6 M. Vanags, A. Šutka "S-7 Elektroķīmiskās un gāzu analīzes metodes gaismas jutības īpašību pētīšanai fotokatalītiskiem materiāliem"
2. S-7 M. Vanags, A. Šutka "Tīra un modificēta hematīta Fe2O3 plānu kārtiņu fotoelektroķīmisko īpašību pētījumi"
3. S-8 M. Vanags, J. Kleperis, G. Bajārs "V-A līkņu metodes pielietošana procesu efektivitātes noteikšanai impulsu un līdzstrāvas ūdens elektrolīzē

5th Topical Meeting of the International Society of Electrochemistry: Interfacial Electrochemistry at Atomic, Molecular and Nanoscale. April 28-30, 2014, Niagara Falls, Canada:
4. Martins Vanags, Gunars Bajars, Andris Sutka, Liga Grinberga, Janis Kleperis, Ineta Liepina. Photocatalytic Activity of Ferrite Based Nanoparticles, Their Clusters and Thin Films for Solar Water Splitting.

2013.g.
Int. Conf. ''Functional materials and nanotechnologies 2013'' Tartu, Estonia in April, 21 – 24, 2013:
5. PO-53 Vanags M, Kleperis J, Bajars G, Nemcevs V. "Electrodeposition of Nanoporous Nickel Layers Using Inductive Voltage Pulses" Abstr. Int. Conf. ''Functional materials and nanotechnologies 2013'' Tartu, Estonia in April, 21 – 24, 2013,, p.158

2012.g.

28th Scientific Conference of Institute of Solid State Physics University of Latvia. February 8-10, 2012, Riga

6. P.Aizpurietis, M.Vanags, J.Kleperis. Electrolysis efficiency studies of steel electrodes with Raney nickel plating, p.47.

Int.Conf. "Functional materials and nanotechnologies" FM&NT-2012. Riga

7. M.Vanags, P.Aizpurietis, J.Kleperis, G.Bajars. Comparison of Electrodes with Smooth and Nanostructured Surfaces in Pulse and D Electrolysis. In: Abstr.. 2012. PO-183, P.296.

2011.g.

The 27th Scientific Conference of Institute of Solid State Physics of University of Latvia, Riga, February 14 – 16, 2011,

8. M.Vanags, G.Bajars, J.Kleperis, A.Lusis, Cathode and Anode Behaviour During Pulsed DC Electrolysis of Water. Abstracts p. 13.
9. J.Kleperis, M.Vanags, Y.Kuznecov, P.Liopa, Construction of Microcapillary and Ionization Devices for Production of Combustible Gas Mixtures to be Used on Site, 2011, p. 34.

International Conference FM&NT Functional Materials and Nanotechnologies 2011, ISSP University of Latvia, Riga, April 5-8.2011

10. M.Vanags, J.Kleperis, G.Bajars, A.Lusis. Description of Model and Verification Eksperiments for Hydrogen Evolution Reaction: Dependence on Electrode Material. Book of Abstracts of, 2011, PO-137, p. 230

1th International Congress on Hydrogen Production ICH2P-11, Thessaloniki, Greece, June 19-22,

11. J.Kleperis, M. Vanags, G. Bajars. Current Behaviour During Pulsed Dc Electrolysis Of Water. Paper No 266ELE;; Conference Abstracts Proceedings in CD form, 2011, 5 pages;

4th World Hydrogen Technology Convention, 14th-16th September 2011 Scottish Exhibition and Conference Centre, Glasgow, Scottland, UK

12. M. Vanags, J. Kleperis, G. Bajars, A. Lusis. Analysis Of Inductive Current Pulse Dynamics In Water Electrolyses Cell. Conference Abstracts p.68;

2010.g.

The 26th Scientific Conference of Institute of Solid State Physics of University of Latvia, Riga, February 14 – 16, 2011:

13. M. Vanags, G. Bajārs, J. Kleperis, Elektrolīzes reakcijas norisei nepieciešamās sliekšņa enerģijas nosacījumi un tās samazināšanas iespējas. Tēžu krājums, lpp. 76.
14. J. Blūms, M. Vanags, J. Kleperis, Temperatūras ietekme uz ģenerēto jaudu rūpnieciskiem Saules fotoelektriskajiem paneļiem. Tēžu krājums, lpp. 79.

International Conference „Functional Materials and Nanotechnologies" FM&NT 2010, March 16-19, 2010, Riga (Latvia):

15. J.Kleperis, M.Vanags, J.Hodakovska, J.Klavins. Oriented Nanostructures for Solar-Hydrogen Technologies. Abstracts of, p. 82
16. M. Vanags, J.Kleperis, G. Bajars. Short Duration Voltage and Current Transients on Water Electrolysis Cell. Abstracts, p. 129.

7th International Conference Of Young Scientists On Energy Issues Cyseni 2010; May 26-27, 2011, Lithuanian Energy Institute, Kaunas, Lithuania:

17. M. Vanags, J. Kleperis, G. Bajars. Water electrolyses powered with inductive spikes. Abstract 1 page.
18. J. Blums, M. Vanags, J. Kleperis. Effect of ambient temperature on commercial photovoltaic solar cells. Abstract 1 page.

9th International Symposium on Systems with Fast Ionic Transport (9th ISSFIT), June 1 – 5, 2010, Riga, University of Latvia (Latvia):

19. M. Vanags, G. Bajars, J. Kleperis, A. Lusis Peculiarities of short pulse water electrolysis: Ion transport and discharge at electrodes. Abstracts of, p. 133.

61st Annual Meeting of the International Society of Electrochemistry „Electrochemistry from Biology to Physics", September 26 - October 1, 2010, Nice (France):

20. Martins Vanags, Janis Kleperis, Gunars Bajars, Andrejs Lusis. Peculiarities of water electrolysis with high voltage short pulses. Abstracts of Format CD, 1 page.

VI Российская Конференция "Физические проблемы водородной энергетики" 22–24 ноября 2010 года; Физико-технический институт им. А.Ф. Иоффе РАН, Санкт-Петербург, Россия. 6th Russian Conference „Physical Problems of Hydrogen Energetics", November 22-24, Saint Petersburg (Russia"):

21. G. Bajars, M. Vanags and J. Kleperis. Efficiency Improvement of Water Electrolysis for Hydrogen Production. Abstracts of, p.20.

2009.g.

The 25th Scientific Conference of Institute of Solid State Physics of University of Latvia, Riga, February 14 – 16, 2011:

22. I. Dirba, M. Vanags, J. Kleperis, Hydrogen Usage in an Internal Combustion Engines – description and optimisation of burning. Abstracts, p. 44.

Baltic Sea Region Conference "Functional materials and nanotechnologies" FM&NT-2009, Riga, March 31 - April 3, 2009:

23. V. Kuzmovs, J. Kleperis, M. Vanags, G. Bajars, K. Garkevics, Structural and Morfological Research of Lead/Acid Battery Plates: Pulse Charge Effect. Abstracts of International, p. 205.
24. M. Vanags, I. Klepere, G. Bajars, G. Chikvaidze, J. Kleperis, Kinetics of Hydrogen Evolution Reaction on Cathode – Electrolysis Model development and testing with Microrespiration Sensors. Abstracts, p. 208.;

6th International Conference of Young Scientists on Energy Issues CYSENI 2009, May 27-28, 2009, Kaunas, Lithuania:

25. M. Vanags, J. Kleperis, G. Bajars, G. Vaivars. Water electrolysis – traditional and uncommon aspects. The. Abstracts Online: http://www.cyseni.com/2009/content/view/53/1/lang,en/

ICHMS'2009 XI International Conference, Yalta, Ukraine, August 25-31,2009

26. M.Vanags, J.Kleperis, G.Bajars, „Electrolysis model development for metal electrolyte interface: testing with microrespiration sensors", Extended Abstracts, 4 pages.

2008.g.

The 24th Scientific Conference of Institute of Solid State Physics of University of Latvia, Riga, February 14 – 16, 2011:

27. M. Vanags, V. Nemcevs, J. Kleperis, Water electrolysis with high voltage and high frequency method. Abstracts, p. 36.

International conference "Eco-Balt 2008" May 15-16, 2008, Riga (Latvia):

28. M. Vanags, J. Kleperis, Water splitting into hydrogen and oxygen using water dielectric properties; Abstracts of, p.19.

5th Baltic Conference on Electrochemistry (BEC-5) Tartu, Estonia, April 30 – May 3, 2008

29. M. Vanags, G. Bajars, J. Kleperis, A. Lusis. Influence of high voltage AC and magnetic field on water electrolysis. Abstracts, p.145.

2007.g.

Annual 23rd Conference of Institute of Solid State Physics of University of Latvia, February 13-15, 2007, Riga, Latvia:

30. J. Blums, M. Vanags, J. Kleperis, Water electrolysis at different current – voltage regimes. Abstracts of, p. 54.
31. M. Vanags, V. Nemcevs, J. Kleperis, Classical and unconvential aspects of water electrolysis. Abstracts, Riga, Latvia, p. 57.

International Baltic Sea Region Conference "Functional materials and nanotechnologies" FM&NT-2007, Riga, April 2-4, 2007:

32. M. Vanags, J. Kleperis, G. Bajars, A. Lusis, Water electrolysis using electrodes with modified surface/volume. ABSTRACTS, p. 44.
33. **International conference "Eco-Balt 2007" May 10-11, 2007, Riga (Latvia):**

Martins Vanags, Janis Kleperis, Position of hydrogen energy in Latvian economics; Ūdeņraža enerģētikas vieta Latvijas ekonomikā, Abstracts, p.109.

2nd International Hydrogen Energy Congress and Exhibition IHEC 2007; Istanbul, Turkey, 13-15 July 2007:

34. Martins Vanags, Peteris Shipkovs, Janis Kleperis, Gunars Bajars and Andrejs Lusis. Water electrolysis: unconvential aspects.